Accepted Manuscript

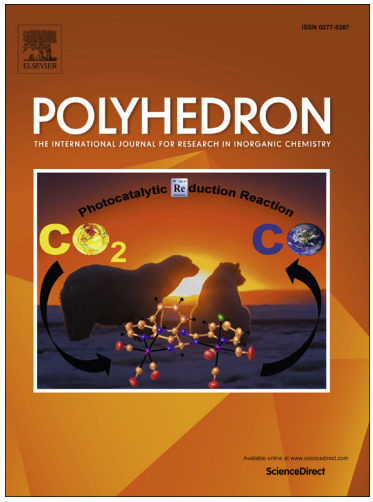

DNA / protein binding, cytotoxicity and catecholase activity studies of a piperazinyl moiety ligand based nickel(II) complex

Soumen Mistri, Horst Puschmann, Subal Chandra Manna

PII: S0277-5387(16)30143-7
DOI: http://dx.doi.org/10.1016/j.poly.2016.05.003
Reference: POLY 11974

To appear in: *Polyhedron*

Received Date: 29 February 2016
Accepted Date: 1 May 2016

Please cite this article as: S. Mistri, H. Puschmann, S.C. Manna, DNA / protein binding, cytotoxicity and catecholase activity studies of a piperazinyl moiety ligand based nickel(II) complex, *Polyhedron* (2016), doi: http://dx.doi.org/10.1016/j.poly.2016.05.003

DNA / protein binding, cytotoxicity and catecholase activity studies of a piperazinyl moiety ligand based nickel(II) complex

Soumen Mistri,[a] Horst Puschmann,[b] Subal Chandra Manna[*,a]

[a] *Department of Chemistry & Chemical Technology, Vidyasagar University, Midnapore 721102, West Bengal, India, E-mail: scmanna@mail.vidyasagar.ac.in, Fax: (91) (03222) 275-329.*

[b] *Department of Chemistry, University of Durham, South Road, Durham DH1 3LE, U.K.*

ABSTRACT

The Ni(II) complex, {[Ni(HL)$(SCN)_2(H_2O)$]·2(DMF)} (**1**) [HL=6-methoxy-2-{[2-(1-piperazinyl)ethylimino]methyl}phenol], was synthesized and characterized by X-ray crystal structure analysis and spectroscopic methods. The crystal structure of complex **1** reveals a distorted octahedral coordination geometry around the nickel centre which forms a supramolecular assembly through hydrogen bonds. The interaction of complex **1** with the calf thymus DNA (CT-DNA) was investigated using electronic absorption and fluorescence spectroscopic methods. The results show that complex **1** has binding affinity to CT-DNA in the order of 6.06×10^5 M^{-1}. The interactions of complex **1** with bovine serum albumin (BSA) and human serum albumin (HSA) were also studied using electronic absorption and fluorescence spectroscopic techniques and the analysis show that interaction of complex **1** with BSA/HSA occur mainly with ground state association process. The number of binding sites and binding constant were calculated using double logarithm regression equation. Anticancer activity of **1** in human breast (MCF7) cancer cell lines reveals dose dependent suppression of cell viability with IC_{50} value 64 ± 3.7 μM. Catecholase activity of **1** has been investigated in methanol medium using 3,5-di-*tert*-butylcatechol (3,5-DTBC) as model substrate and the result shows that **1** is active for catalyzing aerobic oxidation of 3,5-DTBC to 3,5-di-*tert*-butylbenzoquinone (3,5-DTBQ).

Keywords: Ni(II) complex; crystal structure; DNA binding studies; serum albumin binding studies; catecholase activity.

1. Introduction

Transition metal coordination compounds are attracting considerable interest due to their potential applications in the field of catalysis [1a-1d], magnetism [1e-1g], fluorescence sensing [1h,1i], medicinal chemistry [1j-1l], etc. Some Schiff-base transition metal coordination compounds play an important role in biology due to their antimicrobial [2], antifungal [3], antibacterial [4], antitumor [5], antiviral [6], antipyretic [3a] and antidiabetic activities [7]. There are reports in the literature that many transition metal complexes may potentially be used as therapeutic agents for the treatment of several human diseases including diabetes, neurological disorders, anti-inflammatory, carcinomas and lymphomas. In addition to this therapeutic application, these compounds also function as potential free radical scavengers and hence behave like anti-oxidant agents [2, 8]. Complexes of vanadium and zinc (antidiabetic agents), platinum and ruthenium (anti-cancer agent), iron, copper and manganese (anti-oxidant and superoxide dismutase mimetic agents) are widely considered in the development of new metallopharmaceutics [9]. Limited numbers of mono / dinuclear Ni(II) complexes have also been reported in the literature and are showing important biological activities: they can strongly bind to and cleave DNA, show dominant anticancer activities and can control apoptosis [10].

Study of the interactions of DNA with transition metal coordination compounds under physiological conditions is important for the design of new metallo-pharmaceuticals. These compounds have the potential to promote oxidative damage to the 2-deoxyribose moiety and / or to nucleo base in presence of oxidizing or reducing agent, redox active metal centre or light [11]. On the other hand, serum albumin is the major soluble protein in the circulatory system

and functions as a transporter and disposer of many endogenous and exogenous compounds like fatty acids, amino acids, drugs, and pharmaceuticals, etc. [12]. Analysis of the kinetics of interactions of DNA / serum albumin and transition metal complex is important to determine the affinities of complex to DNA / protein, and this information will help to develop efficient metallo-pharmaceuticals.

In the present contribution we report the kinetics of the interaction of {[Ni(HL)$(SCN)_2(H_2O)$]·2(DMF)} (**1**) [HL = 6-methoxy-2-{[2-(1-piperazinyl)ethylimino]methyl}phenol] with calf thymus DNA (CT-DNA) and serum albumin. As human serum albumin (HSA) is structurally homologues to bovine serum albumin (BSA), we have taken both the serum albumin for the purpose of analysis. We have also studied anti-cancer and catecholase activities of complex **1**.

2. Experimental section

2.1. Materials and methods

High purity 2-ethylaminopiperazine and 3,5-di-tert-butylcatecholwas purchased from the Aldrich Chemical Co. Inc. and were used. All other chemicals were of AR grade. Solvents used for spectroscopic studies were purified and dried by standard procedures before use [13].

Elemental analyses (carbon, hydrogen and nitrogen) were performed using a Perkin-Elmer 240C elemental analyzer. IR spectra were recorded as KBr pellets on a Bruker Vector 22FT IR spectrophotometer operating from 400 to 4000 cm^{-1}. ESI-MS spectra were recorded on a JEOL MS 700 mass spectrometer in fast atom bombardment (FAB) mode. NMR spectra of ligand recorded on Bruker 400 MHz instrument. Electronic absorption spectra were obtained with Shimadzu UV-1601 UV-vis spectrophotometer at room temperature. Quartz cuvettes with a 1 cm path length and a 3 cm^3 volume were used for all measurements. Emission spectra were recorded on a Hitachi F-7000 spectrofluorimeter. Room temperature

(300 K) spectra were obtained in methanol solution using a quartz cell of 1 cm path length. The slit width was 2.5 nm for both excitation and emission.

The fluorescence quantum yield was determined using phenol as a reference and water medium for phenol. The solvent used for complex is water [refractive index (η), 1]. Emission spectra were recorded by exciting the complex and the reference phenol at the same wavelength, maintaining nearly equal absorbance (~0.1). The area of the emission spectrum was integrated using the software available in the instrument and the quantum yield was calculated [14] according to the following equation:

$$\Phi_s = \Phi_r \frac{A_s}{A_r} \frac{I_r}{I_s} \frac{\eta_s^2}{\eta_r^2}$$

Where Φ_s and Φ_r are the fluorescence quantum yield of the sample and reference, respectively. A_s and A_r are the respective optical densities at the wavelength of excitation, I_s and I_r correspond to the areas under the fluorescence curve; and η_s and η_r are the refractive index values for the sample and reference, respectively.

2.2. Synthesis of 6-methoxy-2-{[2-(1-piperazinyl)ethylimino]methyl}phenol (HL)

A methanolic solution (20 mL) of mixture of 2-hydroxy-3-methoxybenzaldehyde (0.152 g, 1 mmol) and 2-ethylaminopiperazine (1.292 g, 1 mmol) was refluxed for 3 h. The resulting yellow color solution cooled to room temperature and solid yellow compound was obtained after evaporation of solvent under reduced pressure. The compound obtained was re-dissolved in DCM/MeCN (1:1) and filtered. The solution was left for slow evaporation at room temperature. After one week, yellow crystals of HL were obtained. $C_{14}H_{21}N_3O_2$: HR-MS: $[M + H]^+$, m/z, 262.1 (100%) calcd: m/z, 263.0. Anal.found: C, 3.90; H, 7.95; N, 15.95; calc.: C, 63.87; H, 7.98; N, 15.96. ^{1}H NMR ($CDCl_3$, 400 MHz, δ, ppm): 8.29 s (1H), 7.12-6.74 m (3H), 4.95 s (1H), 3.81 s (3H), 3.75-3.68 m (2H), 2.70-2.67 m (6H), 2.66-2.51 m

(5H).^{13}C NMR ($CDCl_3$, 400 MHz, δ, ppm): 165.57 s, 148.53 s, 148.27 s, 124.86 s, 122.86 s, 120.80 s, 119.55 s, 58.50 s, 56.31 s, 56.26 s, 55.80 s, 54.60 s.

2.3. Synthesis of complex

The complex has been synthesized by adopting the procedures schematically given in **Scheme I**.

Scheme I. Synthesis of **1**

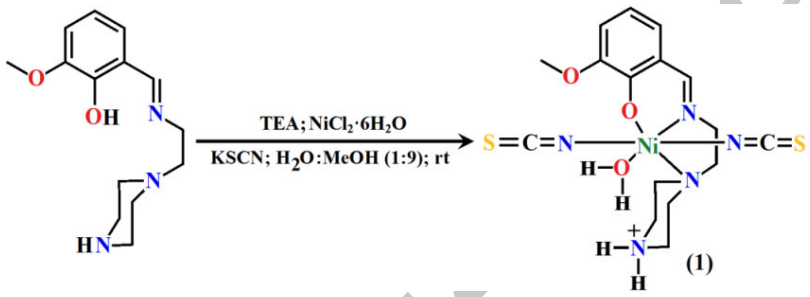

{[Ni(HL)(SCN)$_2$(H$_2$O)]·2(DMF)} (***1***)

A methanolic solution (5 mL) of $NiCl_2·6H_2O$ (1.0 mmol, 0.237 g) was added drop wise to a methanolic solution (10 mL) of mixture of HL (1 mmol, 0.263 g) and Et_3N (1 mmol) with constant stirring at room temperature (25 °C). To the resulting mixture an aqueous solution (1 ml) of KSCN (2mmol, 0.194 g) was added dropwise and resulting green reaction mixture was stirred for 4h at 25 °C and filtered. The filtrate was left for slow evaporation at room temperature. After a few days, green compound was separated and the compound was redissolved in DMF and filtered. Green crystals suitable for X-ray analysis were obtained after two weeks. Yield 75%. Anal.calc. for $C_{22}H_{37}N_7NiO_5S_2$ (602.41): C, 43.82; H, 6.14; N, 16.26. Found: C, 43.80; H, 6.15; N, 16.14 %. The infrared spectrum exhibited the following absorptions (cm^{-1}): 3200-3700 (br,vs), 2975 (s), 2943 (vw), 2092 (s), 1652 (w), 1561 (vs), 1467 (s), 1419 (vs), 1376 (s), 1299 (vs), 1251 (vw), 1124 (vw), 1079 (vs), 1008 (s), 885 (vs), 817 (vs), 652 (s), 509 (s).

2.4. Crystallographic data collection and refinement

X-ray diffraction data of complex **1** were collected at 120 K on an Oxford Diffraction Gemini Ultra diffractometer. Cell refinement, indexing and scaling of the data sets were was performed with the Agilent CrysAlisPro package, Version 1.171.35.10 [15]. The non-standard space group *Ia* was chosen, since it affordas a smaller beta angle than than the standard-setting space group *Cc*. The structure was solved by using ShelXS [16] using direct methods and refined using ShelXL-2014/7 [17] by the full matrix least-squares method based on F^2 with all observed reflections. The terminal S atom of one of the two NCS ligands was modelled as disordered in equal occupancy. The deposited CIF file (CCDC 1021243) contains the full hkl and res files, thereby fully describing the model. All structural work, including the generation of packing diagrams and all geometric calculations were performed using Olex2 [18]. Crystal data and details of refinements are given in Table 1.

2.5. DNA binding experiments

2.5.1. Electronic absorption spectral study

Electronic absorption spectral titration was carried out at a fixed concentration of nickel(II) compound (3 ml, 0.1991M) in water and varying the concentration of CT-DNA from 0 to 4.50 µM. Intrinsic binding constant (K_{ib}) of the complex with CT-DNA was determined using the equation [19]

$$\frac{[\mathrm{DNA}]}{(\varepsilon_a - \varepsilon_f)} = \frac{[\mathrm{DNA}]}{(\varepsilon_b - \varepsilon_f)} + \frac{1}{K_{ib}(\varepsilon_b - \varepsilon_f)}$$

where, [DNA] is the concentration of CT-DNA, ε_a is the extinction co-efficient of the complex at a given CT-DNA concentration, ε_f and ε_b are the extinction co-efficient of the complex, in free solution and when fully bound to CT-DNA, respectively. The plot of $[DNA]/(\varepsilon_a-\varepsilon_f)$ *vs* [DNA] give a straight line with $1/(\varepsilon_b-\varepsilon_f)$ and $1/[K_{ib}(\varepsilon_b-\varepsilon_f)]$ as slope and

intercept, respectively. From the ratio of the slope to the intercept the value of K_{ib} was calculated.

2.5.2. Competitive binding fluorescence measurement

The competitive binding nature of EB and nickel(II) compound with CT-DNA was investigated adopting fluorometric method using aqueous solution of EB bound CT-DNA in HEPES buffer (pH 7.2) at room temperature. In presence of DNA, ethidium bromide (EB) exhibits fluorescence enhancement due to its intercalative binding to DNA. Competitive binding of nickel(II) compound with CT-DNA results fluorescence quenching due to displacement of EB from CT-DNA. The fluorescence intensities at 598 nm (λ_{ex}, 500 nm) of EB bounded CT-DNA with increasing concentration of nickel(II) compound was recorded. The quenching constant (Stern-Volmer constant, K_{sv}) was calculated using Stern-Volmer equation [20]

$$I_0/I = 1 + K_{sv}[complex]$$

where I_0 and I are the emission intensity in absence and in presence of nickel(II) compound, K_{sv} is the Stern-Volmer constant, and [complex] is the concentration of nickel(II) compound.

2.6. Protein binding studies

Stock solutions human serum albumin (HSA) and bovine serum albumin (BSA) were prepared in 55 mM HEPES buffer (pH 7.2). Aqueous solution of the nickel(II) compound was prepared by dissolving the compound in water: HEPES buffer (1:99). The interactions of compound with serum albumins were studied by recording the tryptophan fluorescence of HSA / BSA. To the solutions of serum albumin (3.109 µM, HAS; 8.214 µM, BSA) in 55 mM HEPES buffer (pH 7.2) at room temperature, nickel(II) compound was added, and the

quenching of emission intensities at 344 nm (λ_{ex}, 280 nm) were recorded after gradual addition of 0.1991 M aqueous solution compound.

2.7. Cell Culture

Breast cancer cell line MCF7 was cultured in DMEM medium as monolayers supplemented with 10 % FBS, 100U/ml penicillin and 100 µg/ml streptomycin at 37 °C in a humid condition with 5% CO_2 atmosphere.

2.8. In vitro Cytotoxicity Assay

The cytotoxicity of the compounds was determined by the MTT [3-(4, 5 dimethylthiazol-2-yl)-2-5 diphenyltetrazolium bromide] assay. Cells were seeded at 5 x 10^3 cells per well in 96-well plates. Next day, cells were treated with different concentrations (0.01 – 100 µM) of the compounds for 48 hour. Then, MTT solution was added to each well and further incubated for 3.5 h at 37°C in a humid, 5% CO_2 atmosphere. Finally, medium containing MTT solution was replaced by MTT solvent (4 mM HCl and 0.1% Triton X-100) and incubated for 15 minute at room temperature. The absorbance was read in Thermo Pierce Elisa plate reader at 570 nm. The percentage of growth inhibition was calculated with respect to vehicle (DMSO) treated cells. All the experiments were repeated for three times.

2.9. Immunofluorescence study

For immunofluorescence study cells were seeded on poly-lysine coated cover slip one day prior the treatment. Next day cells were either treated with DMSO or complex for 48 hours. Then cells were washed three times with cold phosphate buffer saline (PBS) followed by fixation with 4% paraformaldehyde at room temperature for 30 minutes. Fixed cells were washed with cold PBS three times, permeabilized with 0.1% Triton X-100 for 10 minutes. Permeabilized cells were blocked with 5% BSA followed by stained with mouse α-tubulin

primary antibody and anti-mouse rodamine conjugated secondary antibody. DNA was stained with DAPI. Fluorescence image was captured using Olympus IX71 microscope.

3. Results and discussion

3.1. Synthetic aspects

The multisite coordinating ligand, HL, was prepared by a onepot synthesis employing condensation of the corresponding amine and aldehyde in methanol under reflux condition, and characterized by NMR (Fig. 1S), ESI mass (Fig. 2S), FT-IR (Fig. 3S), electronic absorption and emission spectra. Using HL, complex **1** was synthesized at room temperature.

3.2. Molecular structure of {[Ni(HL)(SCN)$_2$(H$_2$O)]·2(DMF)}

Crystal structure determination reveals complex **1** consists of discrete molecule, [Ni(HL)(SCN)$_2$(H$_2$O)], and two DMF molecules that are form a hydrogen bond with a metal-bound water molecule. In **1**, HL acts as a meridionally bound tridentate N,N,O donor ligand and the distorted octahedral coordination spere is completed with two N-donor thiocyanate nitrogen and one oxygen from water molecule, resulting in a NiN_4O_2 chromophore. The structure of the metal center with the atom numbering scheme is shown in Figs. 1 and 4S, while selected geometrical parameters are given in Table 2. The nickel(II) center *meridionally* coordinated by the tridentate HL, and completes distorted octahedral coordination sphere with two N-donor thiocyanate nitrogen and one oxygen from water molecule, resulting in a NiN_4O_2 chromophore. The N/O donor [N18, N21, O10] HL and the aqua oxygen O1W define the equatorial plane around each pseudo octahedral nickel ion [Ni1–N18: 2.021(3) A, Ni1–N21: 2.255(3) A, Ni1–O10: 2.024(2) A, Ni1–O1W: 2.121(2) Å]

The *trans* axial positions are occupied by the nitrogen atoms from the two different thiocyanate [Ni1–N1: 2.059(3), Ni1–N2: 2.063(3) Å] with a N1–Ni1–N2 bond angle of

174.13(11)°. Slight distortion of each Ni(II) is also reflected on the *cisoid* angles, which range from 81.78(10) to 97.61(10)°. The equatorial mean plane is slightly distorted (RMSD 0.024) with the metal insignificantly displaced by 0.0368(14) Å towards N2. The packing of structure **1** reveals that each complex forms two hydrogen bonds to the solvate DMF molecules via the metal-bound water molecule [O40–O1: 2.704(3), O1W–O50: 2.796(3) Å]. One of these DMF molecules forms another hydrogen bond through the same oxygen atom to the protonated N atom in a neighboring complex [O50–N24: 2.869(4) Å], which in turn forms another hydrogen bond (through the other H atom) to the phenolic (and M-bound) O atom of the original complex [N24–O10: 2.653(4) Å] (Fig. 2, Table 1S). Fig. 3a and 3b shows the top and side view of the layer respectively.

3.3. ESI mass spectral analysis

The ESI mass spectrometric data for complex **1** was collected in methanol medium and the result is shown in Fig. 5S. Spectrum of complex **1** shows a peak at *m/z* = 456.12, which corresponds to $[Ni(HL)(SCN)_2(H_2O)]^{+}$ (calc. *m/z* = 455.69), indicating that the octahedral coordination environment of Ni(II) in methanol solution is same as in the solid state structure.

3.4. IR spectral results

IR spectra of ligand HL and complex **1** are shown in Figs. 3S and 6S, and the most important absorption bands are summarized in the experimental section and in Table 2S. IR spectra show that ν(O-H) and ν(N-H) stretching vibrations appear in the region 3000-3650 cm^{-1}. Stretching vibrations in the region 2975 – 2992 cm^{-1} are for C_{sp2}–H bond and bands at 2943 – 2965 cm^{-1} are for C_{sp3}–H bond. Aromatic ν(C=C) and aliphatic ν(C=N) stretching vibrations are appears in the region 1419 - 1548 cm^{-1} (for HL) and 1419- 1561 cm^{-1} (for **1**). $\nu_s(C\text{-}O)_{phenolic}$ stretching vibration appears at 1254cm^{-1} (for HL) and 1251cm^{-1} (for **1**),

whereas $\nu(C\text{-}N)_{aliphatic}$ appears at 1082cm^{-1} (for HL) and 1079cm^{-1} (for **1**). For complex **1**, stretching vibrations at 2092 [for ν(CN)], 817 [for ν(CS)] and 509 cm^{-1} [for δ(NCS)] corroborate the presence of N-coordinated thiocyanate ligand [21]. The IR spectrum of **1** shows additional bands corresponding to $\rho_r(H_2O)$ at 767 cm^{-1} and $\rho_w(H_2O)$ at 652 cm^{-1}, indicating the presence of coordinated water molecule.

*3.5. Electronic absorption spectra and fluorescence spectra of complex **1***

Electronic absorption spectrum (Fig. 7S) of 10^{-5} M aqueous solution of complex **1** exhibits bands at 213 nm (0.244 x 10^5 liter mole^{-1} cm^{-1}), 241 nm (0.382 x 10^5 liter mole^{-1} cm^{-1}), 269 nm (0.068 x 10^5 liter mole^{-1} cm^{-1}), 318 nm (0.059 x 10^5 liter mole^{-1} cm^{-1}) and 392 nm (0.035 x 10^5 liter mole^{-1} cm^{-1}). Upon excitation (λ_{ex}) at 269 nm, **1** exhibits fluorescence (λ_{em}) at 313 nm, 328 nm and 360 nm, in aqueous solution at room temperature. Detailed spectral data of HL and complex **1** are summarized in Table 3.

3.6. DNA binding studies

3.6.1. Electronic absorption spectral titration

Hypochromism with or without red / blue shift in the electronic spectra of a compound due to gradual increasing concentration of DNA indicate the intercalation between the compound and DNA [22]. On the other hand hyperchromism is observed in the absorption spectra of a compound with increasing concentration of DNA evidences the non-intercalative interaction between the compound and DNA [23]. In the present study the interaction of Ni(II) compound with CT-DNA was investigated using UV-vis absorption spectral studies. The electronic absorption spectra of complex **1** exhibited bands at 213 nm, 241 nm, 269 nm, 318 and 392 nm. Fig. 4 shows the change in the absorption spectra of aqueous solution of complex **1** (3 ml, 0.1991 M) on gradual addition of 10 µl of aqueous solution (28.181 µM) of CT-

DNA. The absorbance of 275 nm band gradually increases with blue shifting up to 11 nm and finally the band appear at 264 nm. On the other hand the absorbance corresponding to peak at 363 nm gradually decreases. Above change in the electronic absorption spectra indicates that complex **1** bind to the CT-DNA helix via intercalation. The isobestic points at 226 nm, 245 nm and 346 nm in the titration curve (Fig. 4) indicate the presence of more than two species in the medium [24].

Plot of [DNA]/($\varepsilon_a - \varepsilon_f$) vs [DNA] (inset of Fig. 4) is a straight line with $\frac{1}{(\varepsilon_b - \varepsilon_f)}$ and $\frac{1}{K_{ib}(\varepsilon_b - \varepsilon_f)}$ as slope and intercept, respectively. The value of intrinsic binding constant (K_{ib}) was calculated from the ratio of slope to the intercept and calculated value of K_{ib} was 6.06×10^5 L mol^{-1}.

3.6.2. Ethidium Bromide (EtBr) displacement studies

Ethidium bromide (EtBr = 3,8-diamino-5-ethyl-6-phenyl phenanthridinium bromide) shows fluorescence with an orange colour, when it exposed to ultra violet radiation. The intensity of EtBr fluorescence increases around 20 fold in presence of CT-DNA due to strong intercalation of the planar ethidium bromide phenanthridium ring between adjacent base pair of the double helix [11a, 25]. CT-DNA bounded EtBr shows emission at 598 nm on excitation at 500 nm. Addition of a compound, which is capable to interact with CT-DNA, to the solution of a mixture of EtBr-CT-DNA results in the quenching of EtBr-CT-DNA fluorescence intensity. The quenching of fluorescence occurs due to decrease in the number of binding sites on the CT-DNA available for EtBr. The fluorescence quenching observed in presence of compound may be used to study intercalation between CT-DNA and this compound. Fluorescence titration spectra (Fig. 8S) of EtBr-CT-DNA, upon gradual addition of 10 µL 0.1991 M solution of complex **1**, indicates the reduction of fluorescence intensity keeping emission wavelength fixed. This observation suggests that complex **1** displaced EtBr

molecule from the DNA binding sites [25,26]. From the Stern-Volmer equation [20] ($I_0/I = 1 + K_{sv}$[quencher], where I_0 and I are the fluorescence intensity in the absence and in the presence of the quencher, respectively), a linear relationship (Fig. 9S) was obtained from the titration of EtBr-CT-DNA using complex **1** as quencher. The calculated value of binding constant K_{sv} is 44.1753 L mol^{-1}.

3.7. Protein binding studies

Fig. 5 shows the change of electronic absorption spectra of Bovine Serum Albumin (BSA) (3 ml, 8.214 μM aqueous solution) and Human Serum Albumin (HSA) (3 ml, 3.109 μM aqueous solution) in presence of different concentration of complex at pH 7.2 (using HEPES buffer). Electronic absorption spectra of both serum albumins show increase in the absorbance at 280 nm with bathochromic shift (8 nm for BSA; 7 nm for HSA). In addition to this spectral change a new band appears with gradual bathochromic shift for both serum albumins and finally appears at 336 nm and 365 nm for BSA and HSA, respectively. Bathochromic shift at 280 nm confirms the ground state association of complex **1** with serum albumins. The apparent association constants (K_{app}) were calculated adopting the following equation

$$\frac{1}{(A_{obs} - A_0)} = \frac{1}{(A_c - A_0)} + \frac{1}{K_{app}(A_c - A_0)[complex]}$$

where A_{obs} is the observed absorbance at 280 nm of the solution containing different concentrations of the complex, A_0 is the absorbance of serum albumin only and A_c is the absorbance of serum albumin with complex **1**. The calculated values of apparent association constants are 2.29×10^4 L mol^{-1} and 2.43×10^3 L mol^{-1} for **1-BSA** and **1-HSA** complex, respectively.

To examine the interaction of serum albumin (SA) with complex **1**, the fluorescence spectroscopic studies were carried out. In aqueous solution (pH 7.2, HEPES buffer) complex **1** exhibits fluorescence (λ_{em}) at 313 nm, 328 nm and 360 nm at room temperature upon

excitation (λ_{ex}) at 280 nm. On the other hand both BSA and HSA exhibit luminescence at 330 nm, on excitation at 280 nm (in aqueous solution, pH 7.2, HEPES buffer) at room temperature. The change of the fluorescence spectra of BSA [2 ml 8.214 μM (ε at 280 nm 43824$M^{-1}cm^{-1}$) aqueous solution] and HSA [2 ml 3.109 μM (ε at 280 nm 35700$M^{-1}cm^{-1}$) aqueous solution] on the addition of increasing concentration of complex **1** are shown in Fig. 6. Upon gradual addition of 10 μL 0.1991 M aqueous solution of complex **1** to the solution of serum albumins, significant decrease in fluorescence intensity (up to 64.46 and 43.92 % for BSA and HSA, respectively) observed at 330 nm. The quenching of fluorescence intensity of serum albumin upon addition of complex mainly attributed due to association of serum albumin to complex, serum albumin denaturation or conformational change of the serum albumin [27]. From the Stern-Volmer equation [20] a linear relationship were obtained (R = 0.9984 for BSA curve; R = 0.9924 for HSA curve) for the titration of serum albumin using complex **1** as quencher (Fig. 10S). The calculated values of Stern-Volmer quenching constants (K_{sv}) are 21.72×10^5 L mol^{-1} (for BSA) and 21.54×10^5 L mol^{-1} (for HSA). The k_{sv} values indicate that complex **1** has good serum albumin fluorescence quenching ability.

Fluorescence quenching may occur either by dynamic or static mode. In the dynamic quenching process fluorophore and the quencher come into contact during transient existence of the excited state. Whereas in case of static quenching the ground state complex formation occurs between fluorophore and quencher. UV-vis absorption spectral study is the important tool to determine the nature of quenching. From the UV-vis spectral study it is found that the absorption spectra of BSA/HSA influenced by the addition of complex **1**. This phenomenon evidence the existence of static interaction between BSA/HSA and complex **1**.

When a small molecule bind independently in a static mode to a macromolecule in its set of equivalent sites, the equilibrium between free and bound molecules is expressed by the Scatchard equation [28]

$$\log\frac{(F_0 - F)}{F} = \log k_b + n\log[\text{complex}]$$

where k_b is the binding constant of complex with serum albumin, n is the number of binding sites per serum albumin molecule. The plot of $\log\frac{(F_0-F)}{F}$ *vs* log[complex] gives a straight line (inset of Fig. 6) with n and $\log k_b$ as slope and the intercept, respectively. Calculated values of k_b and n are given in Table 4. The values of n for BSA and HSA are 1.12 and 1.25, respectively, which indicates the existence of static binding sites in BSA/HSA for complex **1**.

3.8. Cytotoxicity Assay

Cytotoxic effect of the complex **1** was tested using standard MTT assay. Cells were treated with the complex **1** for 48 hours. Results demonstrated that the complex **1** has moderate toxic effect on growth of MCF7 cells (Fig. 7). Complex **1** exhibits 50% growth inhibition at 64 ± 3.7 μM concentration. Further we have studied the cellular morphology of the cells in the absence and presence of this compound by immunefluorescence study. Our result demonstrated that cellular organization of microtubules and DNA are unaffected upon treatment of this compound suggesting that the compound has moderate cytotoxic effect at the cellular level (Fig. 11S).

*3.9. Catechol oxidase study of complex **1***

The catecholase activity of complex **1** has been investigated using 3,5-di-*tert*-butyl catechol (3,5-DTBC) as model substrate in oxygen saturated methanol medium. At room temperature 1×10^{-4} M methanolic solution of complex **1** was added to the 1×10^{-2} M methanolic solution of 3,5-DTBC. The UV-vis spectrum of the mixture was recorded at a five minute interval for up to 1.5 hour. Absorbance of a new band at 400 nm corresponding to 3, 5-di-*tert*-butylquinone (3, 5-DTBQ) [29] was gradually increased after addition of complex **1** to the solution of 3,5-

DTBC (Fig. 8). log $A_\infty /(A_\infty - A_t)$ versus time (t) plot (where A_∞ and A_t are the absorbance at infinite time and 't' time, respectively) gives a straight line (Fig. 9) passing through origin with 4.78×10^{-5} min^{-1} as slope. The rate constant for complex-substrate mixture was determined from the slope of this curve and its calculated value was 4.78×10^{-5} min^{-1}. Fig. 10, shows the change of rate of reaction with concentration of substrate. From this figure it is clear that at low concentration of 3, 5-DTBC a first order dependence of the rate on the substrate concentration was observed, whereas a saturation kinetics was observed at higher concentration of 3, 5-DTBC. We have applied Michaelis-Menten model [30] for this system and the values of Michaelis binding constant (K_M) 0.372 litre/mol, $1/V = K_M/V_{max}[S] + 1/V_{max}$ where [S] is the concentration of substrate.

The kinetic parameters for the oxidation of 3,5-DTBC by **1** are listed in Table 5. The turnover number (K_{cat}), calculated by dividing V_{max} with concentration of complex [30]. The calculated value of turn over number is 7.51 h^{-1}, which is relatively small to those reported values for nickel(II) complexes [30-32].

ESI-MS spectra (Fig. 12S) of a solution containing 1 : 100 mixture of complex **1** and 3,5 DTBC, exhibits a strong peak at m/z = 621.02 and one small peak at m/z = 618.89. On the other hand when a mixture of starch-potassium iodide solution treated with a mixture containing complex **1** and 3,5-DTBC, results blue coloration. But no blue coloration was observed when starch-potassium iodide solution treated with complex **1** or 3,5-DTBC only. This observation indicates that hydrogen peroxide was produced during catalytic oxidation of 3,5 DTBC to 3,5 DTBQ. Probable mechanistic path for the formation of H_2O_2 as by-product during Ni(II) compound catalyzed oxidation of 3,5-DTBC to 3,5-DTBQ was suggested by *Mukhopadhyay et. al.* [32]. Based on the ESI-MS spectral study and considering the formation of H_2O_2 as by-product during the course of reaction, we have proposed a possible mechanism which is shown in Scheme **II**. Here the catalytic process takes place through

radical pathway and the first electron transfer takes place to imine bond of coordinated Schiff-base, and atmospheric oxygen molecules are reduced to H_2O_2. The ESI-MS spectral peak at m/z = 621.02 corresponds to the intermediate **1a** (*calc. m/z* 620.73), whereas the peak at m/z = 621.02 corresponds to intermediates **1b** (*calc. m/z* 619.73) and **1c** (*calc. m/z* 619.73).

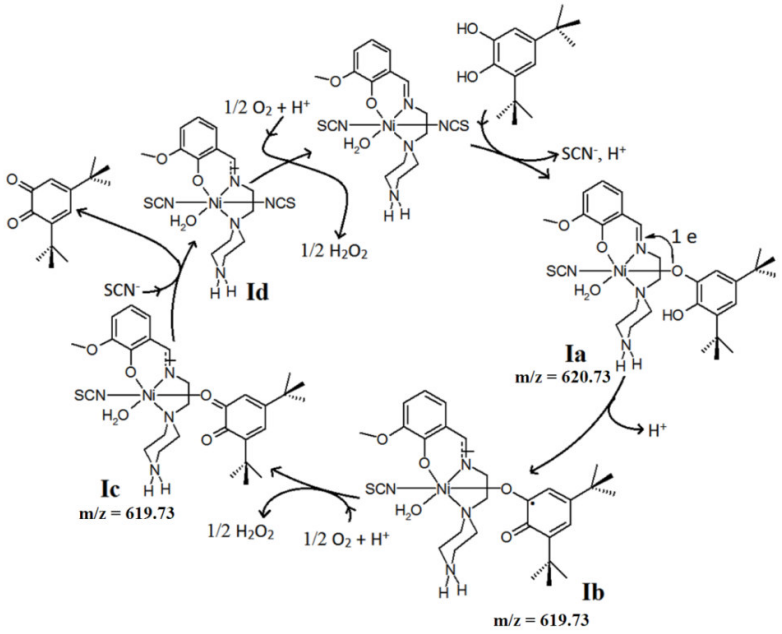

Scheme **II.** Possible mechanism for catalytic oxidation of 3,5-DTBC to 3,5-DTBQ.

4. Conclusion

A nickel(II) complex containing 6-methoxy-2-{[2-(1-piperazinyl)ethylimino]methyl}phenol and thiocyanate ligands was synthesized and characterized by spectroscopic and single crystal X-ray diffraction studies with a view to investigate its biological activity. The nickel complex is mononuclear and extends to a 1D supramolecular chain with hydrogen bonding interactions. The CT-DNA and protein binding of the nickel(II) complex was investigated using electronic absorption and fluorescence spectroscopic techniques. The compound binds effectively to CT-DNA in the order of 10^5 M^{-1} through intercalation. Fluorescence spectroscopic study shows that interaction of complex with serum albumins occur through ground state association process. Cytotoxicity study reveals that the complex shows dose

dependent suppression of human breast (MCF7) cancer cell lines. Nickel(II) complex also exhibits catecholase activity with turnover number 7.51 h^{-1} and probable mechanistic path of catalytic activity has been explained with ESI mass spectroscopy.

Appendix A. Supplementary data

CCDC 1021243 contains the supplementary crystallographic data for complex **1**. This data can be obtained free of charge via http://www.ccdc.cam.ac.uk/conts/retrieving.html, or from the Cambridge Crystallographic Data Centre, 12 Union Road, Cambridge CB2 1EZ, UK; fax: (+44) 1223-336-033; or e-mail: deposit@ccdc.cam.ac.uk. Figures and Tables showing IR, NMR, electronic absorption and fluorescence spectral data are provided as supporting information.

Acknowledgements

The authors gratefully acknowledge the financial assistance given by the CSIR, Government of India, to Dr. Subal Chandra Manna [Project No. 01 (2743)/13/EMR-II]. Authors are also thankful to Dr. Manas Kumar Santra (National Centre for Cell Science, Pune, India) for Cytotoxicity study.

References

[1] (a) M. Eddaoudi, H. Li, O. M. Yaghi, J. Am. Chem. Soc. 122 (2000) 1391-1397; (b) R. Tagore, R. H. Crabtree, G. W. Brudvig, Inorg. Chem. 47 (2008) 1815-1823; (c) J. S. Fossey, R. Matsubara, H. Kiyohara, S. Kobayashi, Inorg. Chem. 47 (2008) 781-783; (d) N. Gharah, S. Chakraborty, A. K. Mukherjee, R. Bhattacharyya, Chem. Commun. (2004) 2630-2632; (e) T. Shiga, K. Maruyama, G. N. Newton, R. Inglis, E. K. Brechin, H. Oshio, Inorg. Chem. 53 (2014) 4272-4274; (f) S. Mistri, E. Zangrando, A. Figuerola, A. Adhikary, S. Konar, J. Cano, S. C. Manna, Cryst. Growth Des. 14 (2014) 3276-3285; (g) S. C. Manna, E. Zangrando, J. Ribas, N. Ray Chaudhuri, Dalton Trans. (2007) 1383-1391; (h) T. Riis-Johannessen, K.

Schenk, K. Severin, Inorg. Chem. 49 (2010) 9546-9553. (i) L. E. McQuade, S. J. Lippard, Inorg. Chem. 49 (2010) 7464-7471; (j) A. Chakraborty, P. Kumar, K. Ghosh, P. Roy, Eur. J. Pharma. 647 (2010) 1-12. (k) B. Duff, V. R. Thangella, B. S. Creaven, M. Walsh, D. A. Egan, Eur. J. Pharma. 689 (2012) 45-55; (l) A. T. Chaviara, P. C. Christidis, A. Papageorgiou, E. Chrysogelou, D. J. Hadjipavlou-Litina, C. A. Bolos, J. Inorg. Biochemistry 99 (2005) 2102-2109.

[2] (a) M. S. Islas, J. J. M. Medina, L. L. L. Tévez, T. Rojo, L. Lezama, M. G. Merino, L. Calleros, M. A. Cortes, M. R. Puyol, G. A. Echeverría, O. E. Piro, E. G. Ferrer, P. A. M. Williams, Inorg. Chem. 53 (2014) 5724-5737; (b) A. Valent, M. Melnik, D. Hudecova, B. Dudova, R. Kivekas, M. R. Sundberg, Inorg. Chim. Acta 340 (2002) 15-20.

[3] (a) A. M. Abu-Dief, I. M. A. Mohamed, Beni-Suef university journal of basic and applied sciences 4 (2015) 119-133; (b) F. Rahaman, B. H. M. Mruthyunjayaswamy, Complex Met. 1 (2014) 88-95.

[4] (a) S. Muche, I. Levacheva, O. Samsonova, L. Pham, G. Christou, U. Bakowsky, M. Hołyńska, Inorg. Chem. 53 (2014) 7642-7649; (b) A. Wojciechowska, A. Gągor, M. Duczmal, Z. Staszak, A. Ozarowski, Inorg. Chem. 52 (2013) 4360-4371; (c) P. K. Panchal, D. H. Patel, M. N. Patel, Synth. React. Inorg. Met. Org. Nano-Met.Chem. 34 (2004) 1223-1235.

[5] (a) D. -D. Yin, Y. -L. Jiang, L. Shan, Chinese J. Chem. 19 (2001) 1136-1140; (b) X. Zhong, J. Yi, J. Sun, H. -L. Wei, W. -S. Liu, K. -B. Yu, Eur. J. Med. Chem. 41 (2006) 1090-1092.

[6] (a) J. Vanˇco, O. ˇSvajlenova, E. Raˇcanska, J. Muselik, J. Valentova, J. Trace Elem. Med. Biol. 18 (2004) 155-161; (b) A. Garoufis, S. K. Hadjikakou, N. Hadjiliadis, Coord. Chem. Rev. 253 (2009) 1384-1397.

[7] J. Vančo, J. Marek, Z. Trávníček, E. Račanská, J. Muselík, O. Švajlenová, J. Inorg. Biochem. 102 (2008) 595-605.

[8] C. Wang, Z. -X. Cai, Z. -L. You, H. -S. Guo, D. -J. Shang, X. -L. Wang, L. Zhang, L. -J. Ma, J. Tan, W. -D. Le, S. Li, Neurochem Res. 39 (2014)1834-1844.

[9] Y. Yoshikawa, H. Yasui, Current Topics in Medicinal Chemistry, 12 (2012) 210-218.

[10] (a) Q. X. Yang, L. Z. Gang, L. W. Sheng, Z. H. Liang, Chin. J. Struct. Chem. 27 (2008) 707-711; (b) C. S. Liu, H. Zhang, R. Chen, X. S. Shi, X. H. Bu, M. Yang, Chem. Pharm. Bull. 55 (2007) 996-1001; (c) P. Krishnamoorthy, P. Sathyadevi, R. R. Butorac, A. H. Cowley, N. S. P. Bhuvanesh, N. Dharmaraj, Dalton Trans. 41 (2012) 4423-4436; (d) S. Poornima, K. Gunasekaran, M. Kandaswamy, Dalton Trans. 44 (2015) 16361-16371.

[11] (a) P. Kumar, S. Gorai, M. Kumar, B. Mondal, D. Manna, Dalton Trans. 41 (2012) 7573-7581; (b) F. Mancin, P. Scrimin, P. Tecilla, U. Tonellato, Chem. Commun. (2005) 2540-2548; (c) M. Pitié, C. J. Burrows, B. Meunier, Nucleic Acids Res. 28 (2000) 4856-4864; (d) B. Maity, M. Roy, S. Saha, A. R. Chakravarty, Organometallics, 28 (2009) 1495-1505; (e) J. A. Cowan, A. Sreedhara, J. Biol. Inorg. Chem. 6 (2001) 337-347; (f) N. H. Williams, B. Takasaki, M. Wall, J. Chin, Acc. Chem. Res. 32 (1999) 485-493; (g) D. S. Sigman, A. Mazumder, D. M. Perrin, Chem. Rev. 93 (1993) 2295-2316; (h) R. Tawa, D. Gao, M. Takami, Y. Imakura, K. -H. Lee, H. Sakurai, Bioorg. Med. Chem. 6 (1998) 1003-1008; (i) M. E. Branum, A. K. Tipton, S. Zhu, L. Que Jr., J. Am. Chem. Soc. 123 (2001) 1898-1904; (j) J. -C. Francois, T. Saison-Behmoaras, C. Barbier, M. Chassignol, N. T. Thuong, C. Héléne, Proc. Natl. Acad. Sci. U. S. A. 86 (1989) 9702-9706; (k) M. P. Fitzsimons, J. K. Barton, J. Am. Chem. Soc. 119 (1997) 3379-3380; (l) R. Hettich, H. -J. Schneider, J. Am. Chem. Soc. 119 (1997) 5638-5647; (m) B. C. Bales, M. Pitié, B. Meunier, M. A. Greenberg, J. Am. Chem. Soc. 124 (2002) 9062-9063.

[12] B. X. Huang, H. Y. Kim, C. Dass, J. Am. Soc. Mass Spectrom.15 (2004) 1237-1247.

[13] D. D. Perrin, W. L. F. Armarego, D. R. Perrin, Purification of Laboratory Chemicals, Pergamon Press, Oxford, U.K., 1980.

[14] J. R. Lakowicz, Principles of Fluorescence Spectroscopy, Third Edition, Springer, New York, USA, 2006.

[15] Aligent (ed) (2010) CrysAlis PRO. Agilent Technologies Ltd, Yarnton.

[16] Sheldrick, G.M., A short history of ShelX, Acta Cryst. A64 (2008) 339-341.

[17] G. M. Sheldrick, Crystal structure refinement with ShelXL. ActaCrystallogr C27 (2015), 3-8.

[18] O. V. Dolomanov, L. J. Bourhis, R. J. Gildea, J. A. K. Howard, H. Puschmann (2009) OLEX2: a complete structure solution, refinement and analysis program. J ApplCrystallogr 42, 339-341.

[19] A. Wolfe, G. H. Shimer, T. Mechan, Biochemistry, 26 (1987) 6392-6396.

[20] J. R. Lakowicz, Principles of Fluorescence Spectroscopy, Third Edition, Springer, New York, USA, 2006.

[21] K. Nakamoto, Infrared Spectra of Inorganic and Coordination Compounds, John Wiley & Sons, New York, 1997.

[22] (a) Q. -L. Zhang, J. -G. Liu, H. Chao, G. -Q. Xue, L. -N. Ji, J. Inorg. Biochem. 83 (2001) 49-55; (b) Z. -C. Liu, B. -D. Wang, B. Li, Q. Wang, Z. -Y. Yang, T. -R. Li, Y. Li, Eur. J. Med. Chem. 45 (2010) 5353-5361.

[23] (a) F. Mancin, P. Scrimin, P. Tecilla, U. Tonellato, Chem. Commun. (2005) 2540-2548;(b) L. Tjioe, A. Meininger, T. Joshi, L. Spiccia, B. Graham, Inorg. Chem. 50 (2011) 4327-4339.

[24] R. K. Gupta, G. Sharma, R. Pandey, A. Kumar, B. Koch, P. -Z. Li, Q. Xu, D. S. Pandey, Inorg. Chem. 52 (2013) 13984-13996.

[25] K. Jeyalakshmi, Y. Arun, N. S. P. Bhuvanesh, P. T. Perumal, A. Sreekantha, R. Karvembu, Inorg. Chem. Front. 2 (2015) 780-798.

[26] (a) J. -B. Lepecq, C. Paoletti, J. Mol. Biol. 27 (1967) 87-106; (b) R. Palchaudhuri, P. J Hergenrother, Current Opinion in Biotechnology, 18 (2007) 497-503; (c) A. J. Geall, I. S. Blagbrough, J. Pharma. Biomed. Analysis, 22 (2000) 849-859; (d) M. A. Kostiainen, J. G. Hardy, D. K. Smith, Angew. Chem. Int. ed. 44 (2005) 2556-2559.

[27] (a) Z. Liu, X. Zheng, X. Yang, E. Wang, J. Wang, Biophysical, 96 (2009) 3917-3925; (b) A. B. T. Ghisaidoobe, S. J. Chung, Int. J. Mol. Sci. 15 (2014) 22518-22538; (c) Y. Wang, G. Zhang, Luminescence, 30 (2015) 198-206.

[28] (a) J. R. Lakowicz, Fluorescence Quenching: Theory and applications, Principles of Fluorescence Spectroscopy, Kluwer Academic/Plenum Publishers, New York, 1999, 53-127;(b) X. -Z. Feng, Z. Lin, L. -J. Yang, C. Wang, C. -L. Bai, Talanta, 47 (1998) 1223-1229.

[29] (a) F. Zippel, F. Ahlers, R. Werner, W. Haase, H. -F. Nolting, B. Krebs, Inorg. Chem. 35 (1996) 3409-3419; (b) A. Biswas, L. K. Das, M. G. B. Drew, C. Diaz, A. Ghosh, Inorg. Chem. 51 (2012) 10111-10121.

[30] (a) P. Seth, L. K. Das, M. G. B. Drew, A. Ghosh, Eur. J. Inorg. Chem. (2012) 2232-2242; (b) P. Kar, R. Haldar, C. J. Gómez-García, A. Ghosh, Inorg. Chem. 51 (2012) 4265-4273.

[31] (a) J. Adhikary, P. Chakraborty, S. Das, T. Chattopadhyay, A. Bauza, S. K. Chattopadhyay, B. Ghosh, F. A. Mautner, A. Frontera, D. Das, Inorg. Chem. 52 (2013) 13442-13452; (b) A. Guha, K. S. Banu, S. Das, T. Chattopadhyay, R. Sanyal, E. Zangrando, D. Das, Polyhedron, 52 (2013) 669-678.

[32] M. Das, R. Nasani, M. Saha, S. M. Mobin, S. Mukhopadhyay, Dalton Trans. 44 (2015) 2299-2310.

Table 1. Crystal data and details of structure refinement of complex **1**.

Complex	**1**
Empirical formula	$C_{22}H_{37}N_7NiO_5S_2$
Formula mass, g mol^{-1}	602.41
Crystal system	Monoclinic
Space group	*Ia*
a, Å	11.6906(5)
b, Å	17.9082(6)
c, Å	14.4741(6)
α, deg	90
β, deg	109.915(5)
γ, deg	90
V, Å^3	2849.0(2)
Z	4
$D_{(calcd)}$, g cm^{-3}	1.404
μ(Mo-Kα), mm^{-1}	0.872
F(000)	1272
Theta range, deg	2.993, 27.999
No. of collected data	18613
No. of unique data	6709
R_{int}	0.042
Observed reflections [$I > 2\sigma(I)$]	6205
Goodness of fit (F^2)	1.045
Parameters refined	356
*R*1, *wR*2 ($I > 2\sigma(I)$) [a]	0.0332, 0.0672
Residuals, e Å^{-3}	-0.36, 0.47

[a] $R1(Fo) = \Sigma \big| |Fo| - |Fc| \big| / \Sigma |Fo|$, $wR2(Fo^2) = [\Sigma w (Fo^2 - Fc^2)^2 / \Sigma w (Fo^2)^2]^{1/2}$

Table 2. Experimental bond distances (Å) and angles (°) for complex **1**.

Bond Distances			
Ni1-O10	2.024(2)	Ni1-N2	2.063(3)
Ni1-O1W	2.121(2)	Ni1-N18	2.021(3)
Ni1-N1	2.059(3)	Ni1-N21	2.255(3)
Bond angles			
N1-Ni1-N2	174.13(12)	N2-Ni1-O1W	85.58(10)
N1-Ni1-N18	92.13(11)	N18-Ni1-N21	81.78(10)
N1-Ni1-N21	94.12(11)	N18-Ni1-O10	90.10(10)
N1-Ni1-O10	89.41(10)	N18-Ni1-O1W	179.10(11)
N1-Ni1-O1W	88.58(10)	N21-Ni1-O10	171.26(10)
N2-Ni1-N18	93.72(11)	N21-Ni1-O1W	97.61(10)
N2-Ni1-N21	87.34(11)	O10-Ni1-O1W	90.46(9)
N2-Ni1-O10	89.96(10)		

Table 3. Photophysical parameters of **1**.

Compound	λ_{ex}, nm (ε_{cal}, $M^{-1}cm^{-1}$)	λ_{em}, nm	$\Delta\nu^a$, nm	φ
1	213 (0.244 x 10^5), 241 (0.382 x 10^5), **269** (0.068 x 10^5), 318 (0.059 x 10^5), 392 (0.035 x 10^5)	313, 328, 360	44, 59, 91	0.125

Bold number indicates the excitation wavelengths. [a]Stoke shift.

Table 4. Kinetic parameters of the interaction BSA /HSA with complex **1**.

Complex-Albumin	T (K)	k_{app} ($Lmol^{-1}$)	n	k_{sv} ($Lmol^{-1}$)	k_b ($Lmol^{-1}$)
1-HSA	300	2.4315×10^3	1.25	21.540×10^5	15.992×10^5
1-BSA	300	22.9494×10^3	1.12	21.720×10^5	12.184×10^5

Table 5. Kinetic parameters for the oxidation of 3,5-DTBC catalyzed by complex **1**.

V_{max} ($M\ min^{-1}$)	Std. error	K_m [M]	Std. error	K_{cat}(h^{-1})	K_{cat}/K_m ($M^{-1}h^{-1}$)
1.252 x 10^{-5}	2.175 x 10^{-6}	0.372	1.02 x 10^{-4}	7.51	28.572

Caption of the Figures

Fig. 1. Ortep view (30%) of complex **1**.

Fig. 2. 1D supramolecular chain of complex **1**.

Fig. 3. (a) Top view of 1D layer of **1**; (b) Side view of 1D layer of **1**.

Fig. 4. Electronic absorption spectra of complex **1** (3 ml, 0.1991 M) in HEPES buffer upon gradual addition of 10 µL 28.181 µM aqueous solution of CT-DNA.

Fig. 5. UV-vis absorption spectra of BSA (3 ml 8.214 µM aqueous solution) (figure **A**) and HSA (3 ml 3.109 µM aqueous solution) (figure **B**) upon gradual addition of 20 µL 0.1991 M aqueous solution of complex **1** at 300K.

Fig. 6. Fluorescence spectra of BSA (2 ml 8.214 µM) (figure **A**) and HSA (2 ml 3.109 µM) (figure **B**) upon gradual addition of 10 µL 0.1991 M aqueous solution of complex **1** at room temperature (λ_{ex} = 280 nm and λ_{em} = 330 nm).

Fig. 7. Dose dependent suppression of cell viability of human breast cancer cell line MCF7 by complex **1**.

Fig. 8. Increase in 3,5-DTBQ band at 400 nm after addition of 10^{-4} M methanolic solution of complex **1** to 100 fold methanolic solution of 3,5-DTBC. The spectra were recorded at an interval of 5 min.

Fig. 9. Change in absorption maxima at 400 nm with time after addition of 10^{-4} M methanolic solution of complex **1** to 100 fold methanolic solution of 3,5-DTBC**.**

Fig. 10. Rate vs. substrate (left) concentration and Lineweaver-Burk (right) plots for complex **1**.

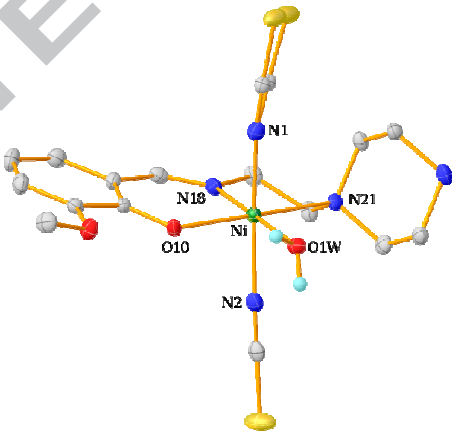

Fig. 1

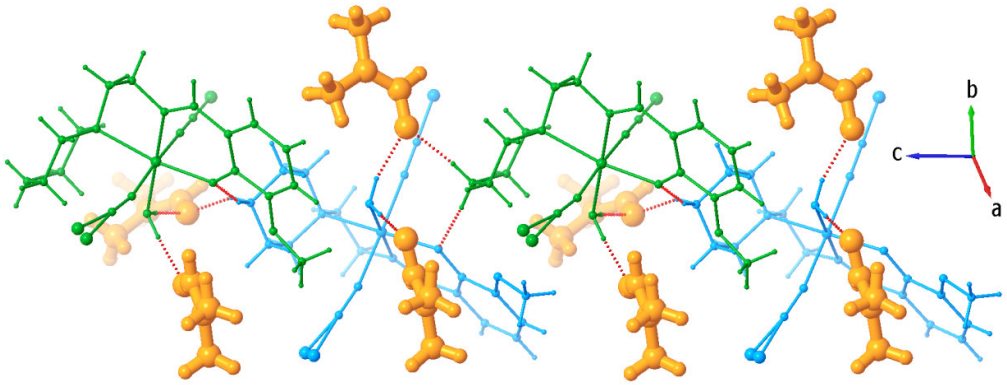

Fig. 2

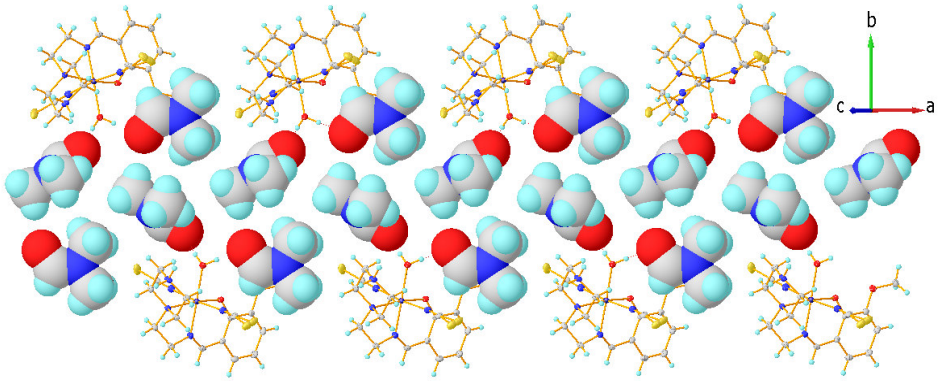

Fig. 3a

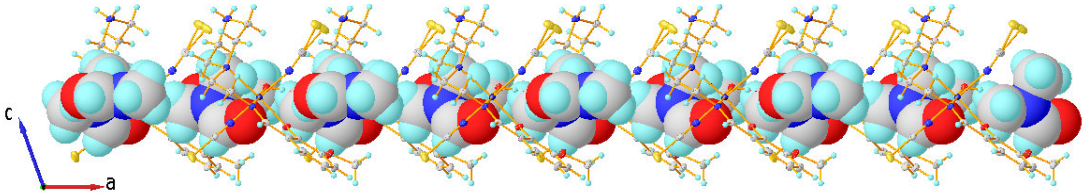

Fig. 3b

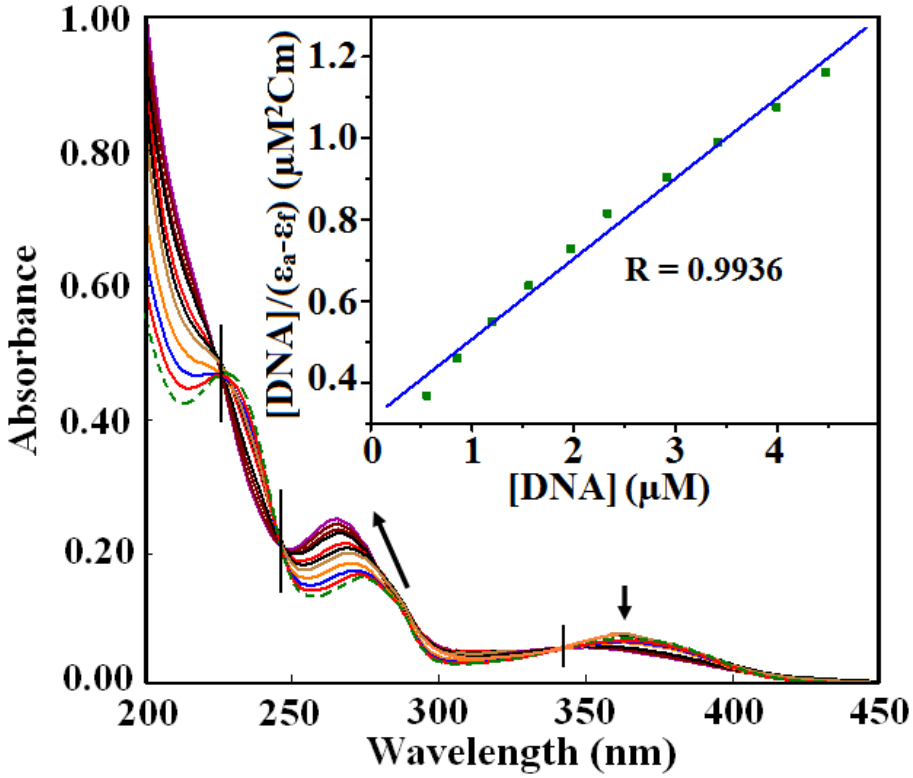
Absorbance
Wavelength (nm)
[DNA]/(εa-εf) (μM²Cm)
[DNA] (μM)
R = 0.9936

Fig. 4

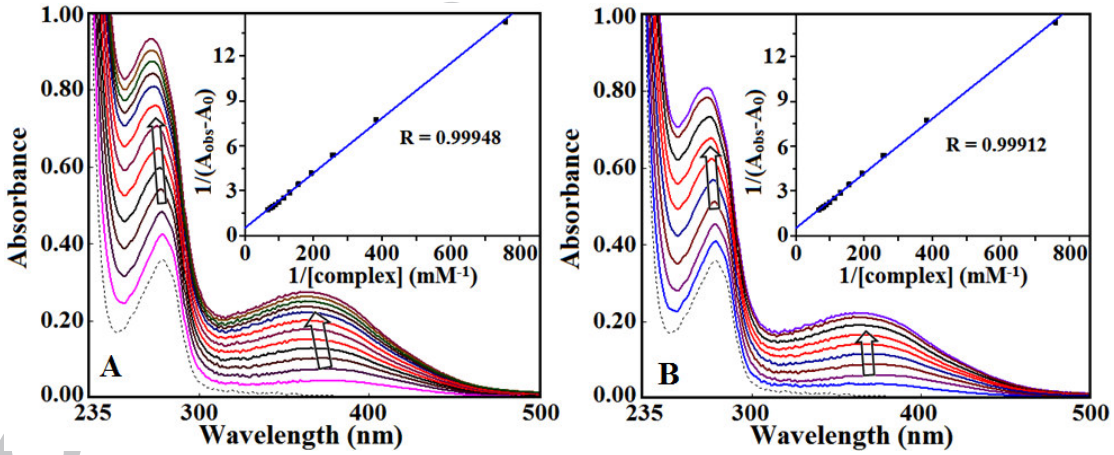
A
B
Absorbance
Wavelength (nm)
1/(Aobs-A0)
1/[complex] (mM⁻¹)
R = 0.99948
R = 0.99912

Fig. 5

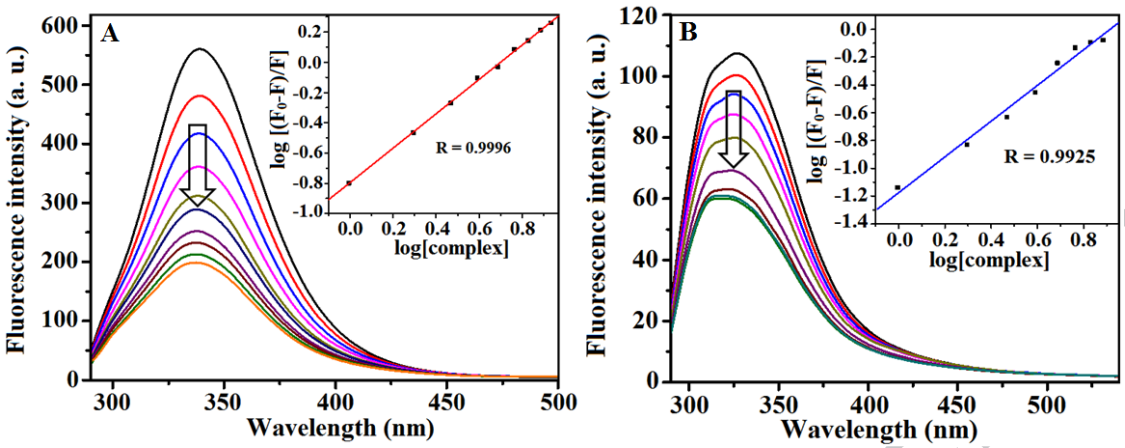
A
Fluorescence intensity (a. u.)
Wavelength (nm)
log [(F0-F)/F]
log[complex]
R = 0.9996
B
Fluorescence intensity (a. u.)
Wavelength (nm)
log [(F0-F)/F]
log[complex]
R = 0.9925

Fig. 6

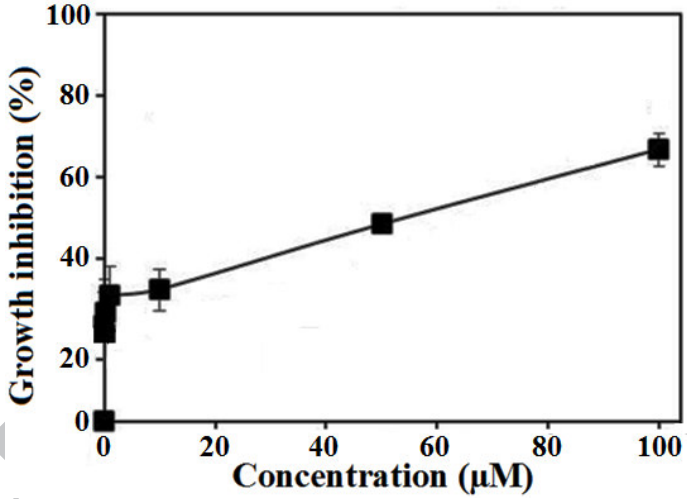
Growth inhibition (%)
Concentration (μM)

Fig. 7

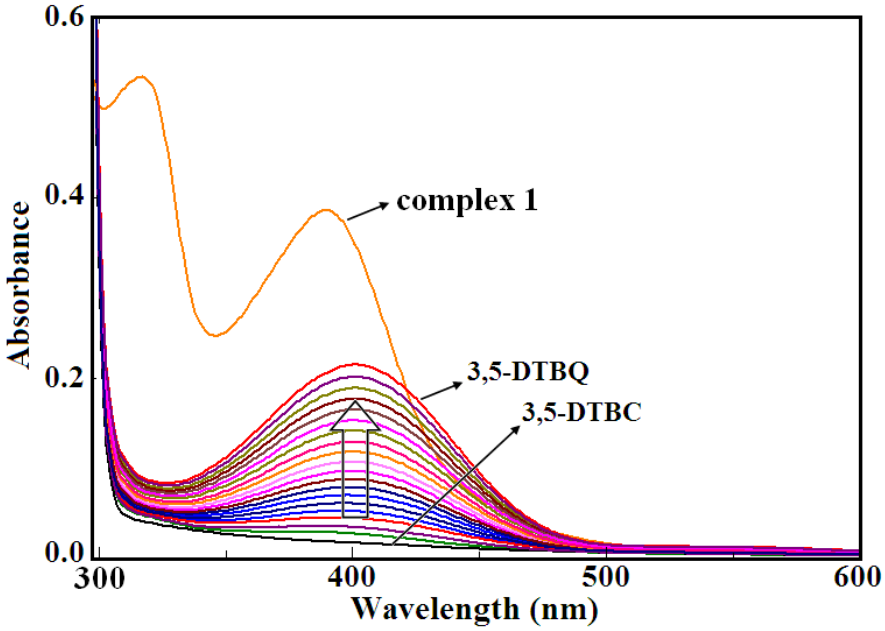
0.6
0.4
0.2
0.0
Absorbance
300
400
500
600
Wavelength (nm)
complex 1
3,5-DTBQ
3,5-DTBC

Fig. 8

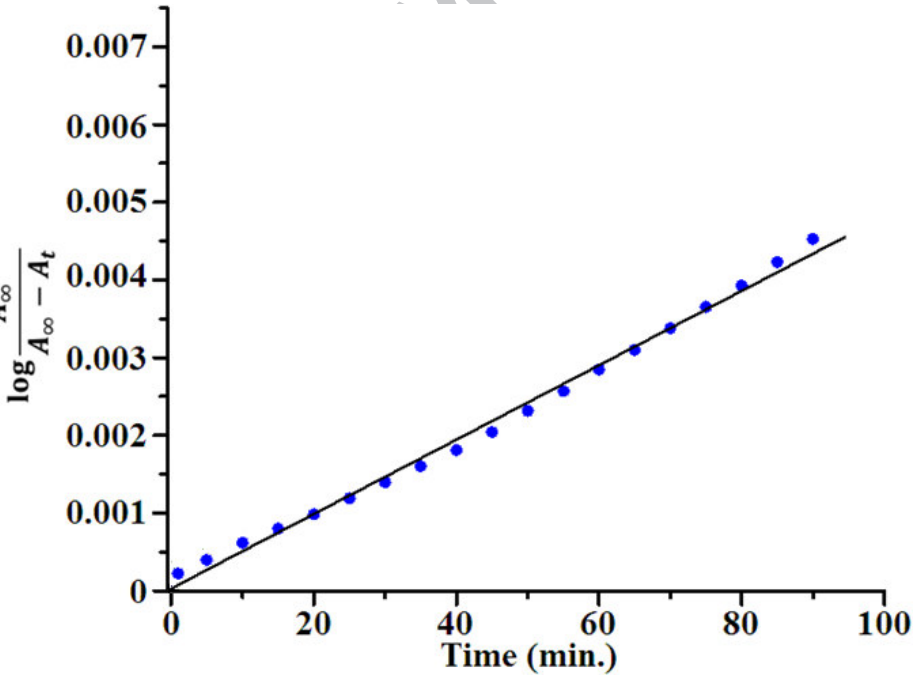
0.007
0.006
0.005
0.004
0.003
0.002
0.001
0
$\log \frac{A_\infty}{A_\infty - A_t}$
0
20
40
60
80
100
Time (min.)

Fig. 9

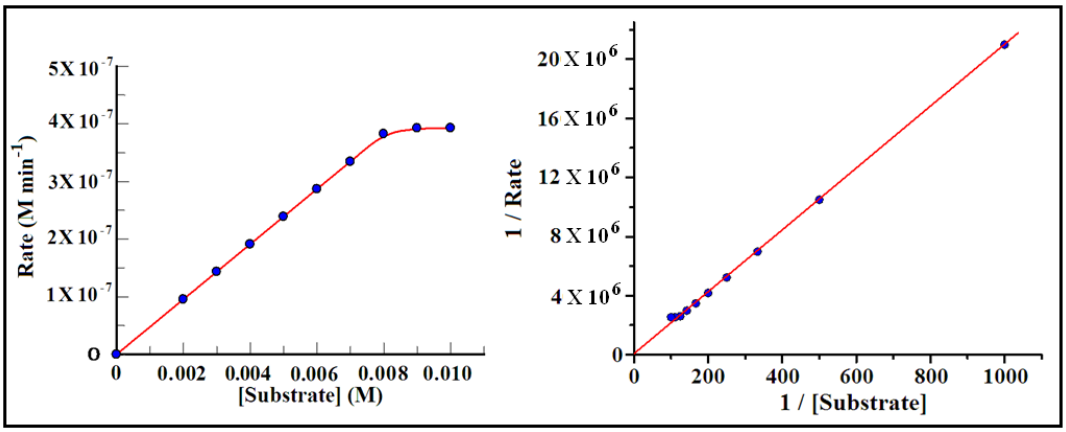

Fig. 10

The interactions of a Ni(II) compound with CT-DNA and serum albumins were studied using electronic absorption and fluorescence spectroscopic techniques. The compound has binding affinity to CT-DNA in the order of $6.06 \times 10^5\ M^{-1}$ and it interact with serum albumins with ground state association process.